Korean J. Chem. Eng., 32(1), 178-183 (2015)
DOI: 10.1007/s11814-014-0265-2

pISSN: 0256-1115
eISSN: 1975-7220

MnO/C nanocomposite prepared by one-pot hydrothermal reaction for high performance lithium-ion battery anodes

Hongyeol Park, Dae Hoon Yeom, Jaegyeong Kim, and Jung Kyoo Lee†

Department of Chemical Engineering, Dong-A University, Busan 604-714, Korea
(*Received 3 April 2014 • accepted 5 September 2014*)

Abstract−Among various candidates to replace the low capacity graphitic carbon anode in current lithium ion batteries (LIBs), manganese oxides possess the advantages of high lithium storage capacity, low cost, high intrinsic density, environmental friendliness and low lithium storage voltage, *i.e.,* 0.5 V Li^+/Li. Manganese oxides, however, have to be incorporated with conducting and porous matrix due to poor electrical conductivity and large volume expansions associated with conversion reaction upon cycling. In this study, a facile one-pot route was attempted for the synthesis of MnO/C nanocomposite for which Mn_3O_4 nanoparticles were grown in aqueous medium followed by carbon gel formation in a one-pot reactor. Thus obtained Mn_3O_4/C carbon gel was transformed into MnO/C nanocomposite by thermal annealing in an Ar flow. The MnO nanoparticles (60 wt%) of 20-50 nm in diameter were well dispersed throughout the MnO/C composite. The MnO/C composite delivered reversible capacity of 541 mAh g^{-1} with an excellent cycling stability over 100 cycles, while parent Mn_3O_4 lost most of its capacity in 10 cycles. The MnO/C composite also exhibited much higher rate capability than a commercial graphite anode. Hence, the MnO/C composite based on low cost materials and facile synthetic process could be an attractive candidate for large-scale energy storage applications.

Keywords: Lithium-ion Battery, Anode, Manganese Oxide, Carbon Composite, Transition Metal Oxide

INTRODUCTION

With the great success of high energy lithium-ion batteries (LIB) in powering small consumer electric devices, LIB technology is being further explored for use in the emerging large scale applications such as various electric vehicles and energy storage system (ESS) for many other applications [1-3]. Compared with the LIB cells for small electronic devices, these emerging large scale applications necessitate more advanced characteristics of LIB, including high energy and power density, low cost material, improved safety and reliability [3-6]. For commercial lithium ion batteries, graphitic carbon has been used as the anodes because of its excellent cycling stability and relatively low cost. However, graphitic carbon offers low theoretical specific (372 mA g^{-1} with one Li per C_6) and volumetric capacities, very poor rate capability due to low intrinsic Li intercalation rate into its lattice crystal structure (d=3.35 Å) raising safety concern at high rate charging due to lithium plating. Hence, the performance of LIB can be further improved by adopting advanced anode material providing higher (volumetric as well as specific) capacity and faster charging capability than graphitic carbon.

Nano-sized transition metal oxides (TMOs), first reported by Piozot et al. in 2000 [7], are promising candidates for anode materials due to their high capacity (750-1,200 mAh g^{-1}) attainable by the "conversion reaction" given in Eq. (1) in which full utilization of all the oxidation states of high-valance transition-metal oxides can be achieved. And reaction (1) is thermodynamically spontaneous in the forward side since the Gibbs free energy changes are in the range of −200~−430 kJ mol^{-1} [14]. The reverse reaction should proceed if an external electromotive force (emf) greater than the equilibrium potential is applied [14]. In addition, TMOs (e.g., FeO_x, MnO_x and etc.) are abundant, cheap and non-toxic and have high intrinsic density (4.9-5.4 g cm^{-3} versus 2.16 g cm^{-3} for graphite) [8-18]. A great attention is being paid to manganese oxides (MnO_x) because 1) MnO_x can store two to eight Li ions per formula unit dependent upon its oxidation state as shown in reactions (2), (3), (4) and (5), corresponding to the theoretical conversion capacities of 756, 1,223, 1,018 and 937 mAh g^{-1}, respectively [15,17-21], and 2) MnO_x possesses much lower equilibrium potential giving lower reduction (charging in a full cell battery) voltage plateau (around 0.5 V vs. 0.8-1.0 V for FeO_x), and thus can offer higher energy density than other TMOs when coupled with specific cathode in a full LIB cell [4,14,15]. Like other TMOs, however, MnO_x has poor electrochemical reversibility due to extremely low electrical conductivity (~10^{-5}-10^{-8} S/cm) and drastic chemical and structural changes inherently accompanying the conversion reactions [13,22,23].

$$M_xO_y+2y\,(Li^+)+2y\,(e^-)\leftrightarrow x\,(M)+y\,(Li_2O) \quad (1)$$

$$MnO+2Li^++2e^-\leftrightarrow Mn+Li_2O \quad (2)$$

$$MnO_2+4Li^++4e^-\leftrightarrow Mn+2Li_2O \quad (3)$$

$$Mn_2O_3+6Li^++6e^-\leftrightarrow 2Mn+3Li_2O \quad (4)$$

$$Mn_3O_4+8Li^++8e^-\leftrightarrow 3Mn+4Li_2O \quad (5)$$

MnO_x are widely used in many industrial applications including catalysts, adsorbents, supercapacitor and cathode material for LIB. MnO_x can be prepared by precipitation [24], hydrothermal

†To whom correspondence should be addressed.
E-mail: jklee88@dau.ac.kr
Copyright by The Korean Institute of Chemical Engineers.

synthesis [25], sol-gel [26] and microwave heating methods [27]. Among various routes to mitigate the inherent problems associated with LIB anode application, MnO_x incorporation into nanostructured composites with conducting matrix such as carbon could be one of the most promising approaches [13,15,17]. For large-scale applications such as ESS and various electrified vehicles, facile and scalable synthetic methods for MnO_x based composite have to be developed.

Herein we report a facile synthesis strategy in which MnO_x nanoparticle formation and carbon gel coating processes are combined in a one-pot reaction to prepare MnO_x/C nanocomposite. This synthesis approach eliminates the conventional processes of separate synthesis of MnO_x nanostructures and additional steps of coating or hybridization with carbon. The as-prepared MnO/C nanocomposite exhibited the reversible capacity of 541 mAh g^{-1} at the current of 100 mA g^{-1} with a remarkable cycling stability over 100 cycles compared with unsupported Mn_3O_4. The MnO/C nanocomposite also showed much higher rate capability than a commercial graphite anode.

EXPERIMENTAL

1. Synthesis and Characterization of MnO_x and MnO/C Nanocomposite

To identify reaction conditions for the formation of manganese oxides, solution phase synthesis of MnO_x was studied first. In a typical synthesis of manganese oxide nanocrystals (Mn_3O_4), 10.1 g of manganese acetate ($Mn(CH_3COO)_2$)·$4H_2O$, ≥99%, Sigma-Aldrich) was dissolved in 14.0 mL of DI water in a glass vial. The mixture was heated and maintained at 100 °C in an oil bath. NH_4OH (28 wt%) solution was added dropwise into the mixture under stirring to maintain its pH at around 9. A small amount of sample was taken after various reaction times: 2, 4, 8 and 16 h. Then, manganese oxide nanocrystals were isolated, washed with DI water and dried at 80 °C in air overnight. Thus obtained manganese oxides were further annealed at 300 °C in an Ar flow for 5 h [28] and were analyzed by XRD to identify their crystal structures.

The MnO_x/C nanocomposites were prepared via one-pot reaction, in which MnO_x nanoparticle formation and their carbon gel coating processes were combined, followed by thermal annealing. According to the procedure described above, manganese oxide was first formed in an aqueous solution at 100 °C for 2 h. During the reaction, the pH of reaction mixture was maintained at around 8-9 by stepwise addition of NH_4OH solution. After the reaction, the mixture was cooled to room temperature. Resorcinol and formaldehyde were added as the carbon precursor and dissolved in the mixture for 30 min under stirring. Then, the sealed vial containing the mixture solution was heated and maintained at 80 °C overnight to form MnO_x/C gel composite. The gel composite was filtered and washed with DI water until the pH of filtrate solution become neutral. The washed gel composite was dried at 80 °C overnight followed by thermal annealing at 700 °C under Ar flow for 2 h to obtain the MnO_x/C nanocomposite.

2. Materials Characterization

The powder XRD patterns of samples were recorded on an Ultima IV, Rigaku model D/MAX-50 kV system (Cu-Kα radiation, λ= 1.5418 Å). The carbon content in MnO_x/C composite was determined by the weight loss in a TGA run to 800 °C at a ramping rate of 10 °C min^{-1} in an air flow. The morphology and structure of samples were investigated by using SEM (JEOL JSM-35CF operated at 10.0 kV, JEOL Ltd., Japan) and TEM (JEOL JEM-2010 operated at 200.0 kV, JEOL Ltd., Japan).

3. Electrochemical Measurements

The electrochemical properties were measured using R-2016 coin cell with Li foil as the reference electrode. The working electrodes (35-40 mm thick) were prepared by casting a paste consisting of 80 : 10 : 10 in wt% of active material (Mn_3O_4 or MnO/C composite or graphite), conductive additive (Super P Li, TIMCAL Ltd.) and Poly(vinylidenefluoride) (PVDF) binder, respectively, on a copper foil. Graphite was tested as a reference anode material in comparison to manganese oxide-based materials. The typical coating density of electrodes was 2-3 mg cm^{-2}. A polypropylene membrane (Celgard 2400) was used as the separator and 1.0 M $LiPF_6$ dissolved in an ethylene carbonate/dimethyl carbonate/diethyl carbonate (EC/DMC/DEC) mixture (3 : 4 : 3 v/v/v) (Panax Etech Ltd., Korea) as the electrolyte. The cells were assembled in an argon-filled glove box. Cyclic voltammograms were recorded in the voltage range of 3.0-0.01 V vs. Li^+/Li at the scan rate of 0.1 mV s^{-1}. The cycling tests were conducted in the cut-off voltage range of 0.01-3.0 V vs. Li^+/Li on a galvanostat/potentiostat system (WonATech, Korea).

RESULTS AND DISCUSSION

Fig. 1(a) shows the XRD patterns of MnO_x crystals obtained at

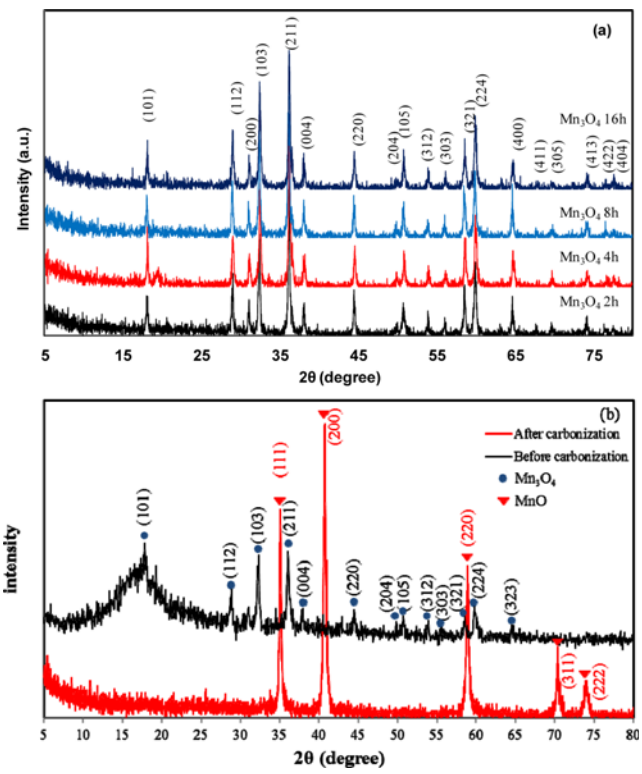

Fig. 1. XRD patterns of (a) Mn_3O_4 obtained at different reaction times of 2, 4, 8 and 16 h, respectively, and (b) MnO_x/C before and after carbonization.

different reaction time. Under the reaction conditions employed in this study, all the diffraction peaks of MnO_x samples could be indexed to the tetragonal Mn_3O_4 structure consistent with the JCPDS data (no. 24-0734) [15]. The crystallinity of Mn_3O_4 particles was about the same for the samples obtained at the time frame of 2-16 h. The result supports that the tetragonal Mn_3O_4 particles can be readily formed at a moderate temperature under slightly basic aqueous condition. The XRD patterns of MnO_x/C composites before and after carbonization at 700 °C under Ar flow are shown in Fig. 1(b). The MnO_x phase in the as-prepared MnO_x/C composite before carbonization was found to be mostly Mn_3O_4 structure, indicating that the crystal structure of tetragonal Mn_3O_4 was maintained during the subsequent carbon gel coating with resorcinol and formaldehyde. After carbonization of Mn_3O_4/carbon gel composite, however, the XRD peaks assignable to MnO only were observed while the broad hump between 2θ=12-25° in the Mn_3O_4/carbon gel decreased substantially due to the enhanced ordering of carbon after carbonization. This result suggests that Mn_3O_4 is reduced to MnO possibly by gaseous hydrocarbon by-products and hydrogen released during carbonization process at high temperature. Similar partial reductions of transition metal oxides were reported on α-Fe_2O_3 and Fe_3O_4 during carbon coating process [11,29].

To determine the carbon content in MnO/C composite, TGA was run up to 900 °C in air flow. As shown in Fig. 2, carbon burning starts at 300 °C and completes below 400 °C. In the TGA profile above 400 °C, mass gain is observed due to further oxidation of MnO. From the mass loss in the 300-400 °C range, the carbon content was estimated to be 40 wt% and the rest 60 wt% could be assigned to MnO in the composite.

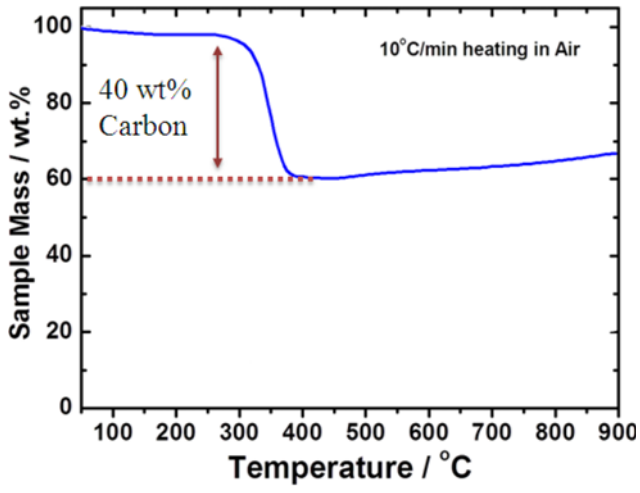

Fig. 2. TGA profile of MnO/C.

The structures of Mn_3O_4 nanoparticles and MnO/C composite were further investigated with TEM. In the TEM images shown in Fig. 3, Mn_3O_4 particles show ellipsoidal-like morphology with rather large sizes of 100-150 nm. In the high magnification image shown in Fig. 3(b), the lattice *d*-spacings of 2.47 and 4.88 Å corresponding to the (211) and (101) planes of Mn_3O_4, respectively, are identified. On the other hand, the MnO particles derived from thermal annealing of Mn_3O_4/carbon gel are much smaller, 20-50 nm, and are evenly dispersed in the carbon matrix as shown in the TEM images in Fig. 4. The reduced size distribution of MnO particles in MnO/C composite could be due to the physical barrier of carbon gel network against particle agglomeration during one-pot synthesis. Hence, the synthesis process employed in this study can provide an efficient method to achieve both the particle growth of transition metal oxides and its encapsulation in carbon matrix in one-pot reaction.

The electrochemical responses of Mn_3O_4 and MnO/C composite measured by cyclic voltammetry (CV) tests for the initial three cycles are given in Fig. 5(a) and 5(b), respectively. In the first cathodic process of Mn_3O_4 electrode, an intense peak was observed between 0.2 and 0.02 V mainly due to the reduction of Mn^{3+} and Mn^{2+} to Mn^0 [21,30]. In the first anodic scan, a small broad peak was observed at 1.15 V corresponding to the oxidation of Mn^0 to Mn^{2+}/Mn^{3+}. In the subsequent cycles, the peak intensity and integrated area of both cathodic and anodic peaks substantially decreased, indicating very poor electrochemical reversibility of Mn_3O_4 [31]. Fig. 5(b) shows the CV profiles of MnO/C composite. In the first cathodic scan, two reduction peaks were recorded at 0.8 V and 0.15-0.03 V. The peak at 0.8 V disappeared in the subsequent cycles suggesting irreversible Li^+ reaction associated with electrolyte decomposition forming a solid-electrolyte interface (SEI) layer [13,28]. The spiky peak at 0.15-0.03 V corresponds to the reduction of Mn^{2+} to Mn^0 and the obvious peak was shifted to 0.37 V in the subsequent cycles due to electrode polarization caused by phase transformation between polycrystalline MnO and Li_2O/Mn nano-domains as observed in the MnO/C system [21,30]. In the anodic scans, the oxidation of Mn^0 to Mn^{2+} appeared at 1.2 V. The redox CV profiles

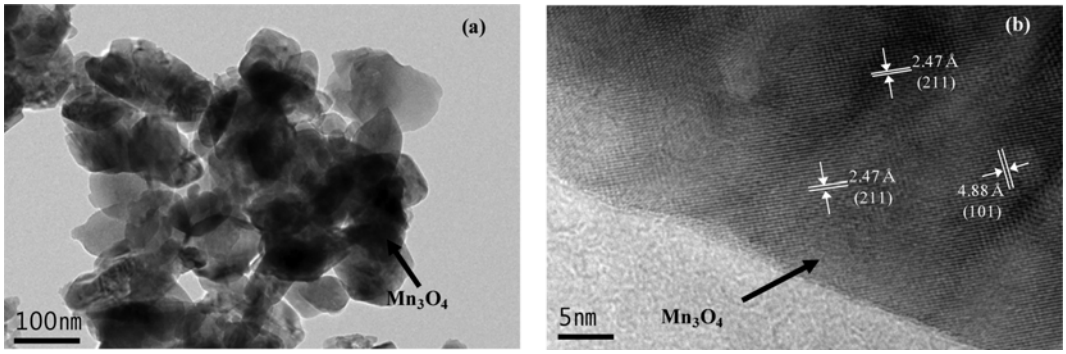

Fig. 3. TEM images of Mn_3O_4 at (a) low and (b) high magnification.

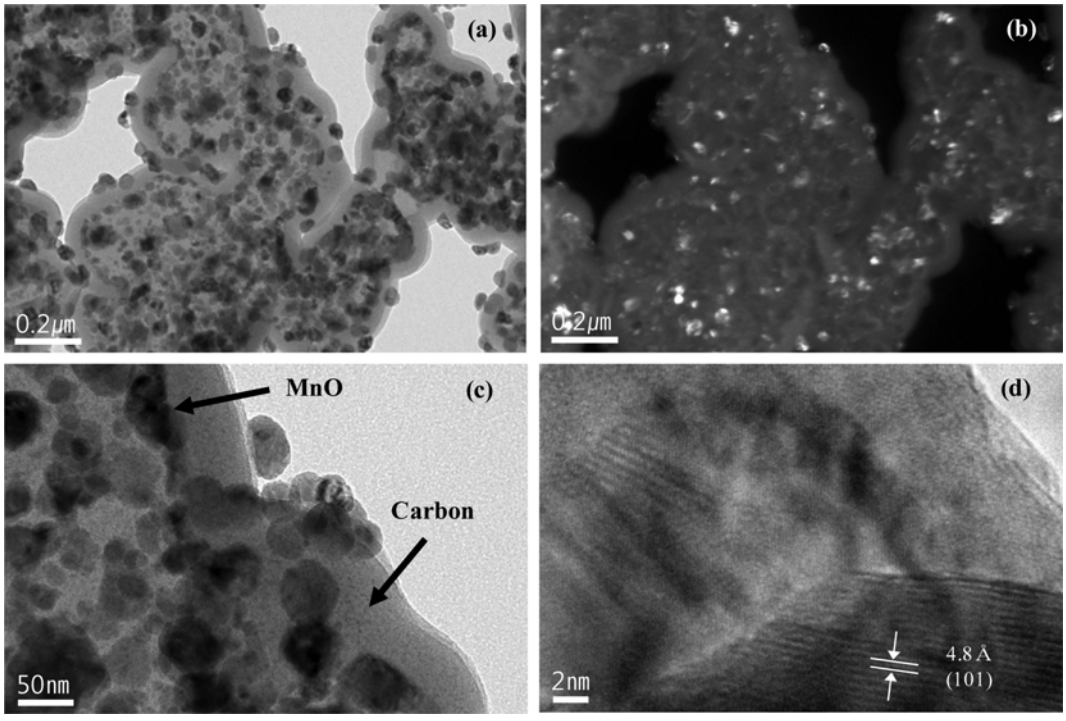

Fig. 4. TEM images of MnO/C nanocomposite; (a), (c) and (d) are bright-field images and (b) is a dark-field image of (a).

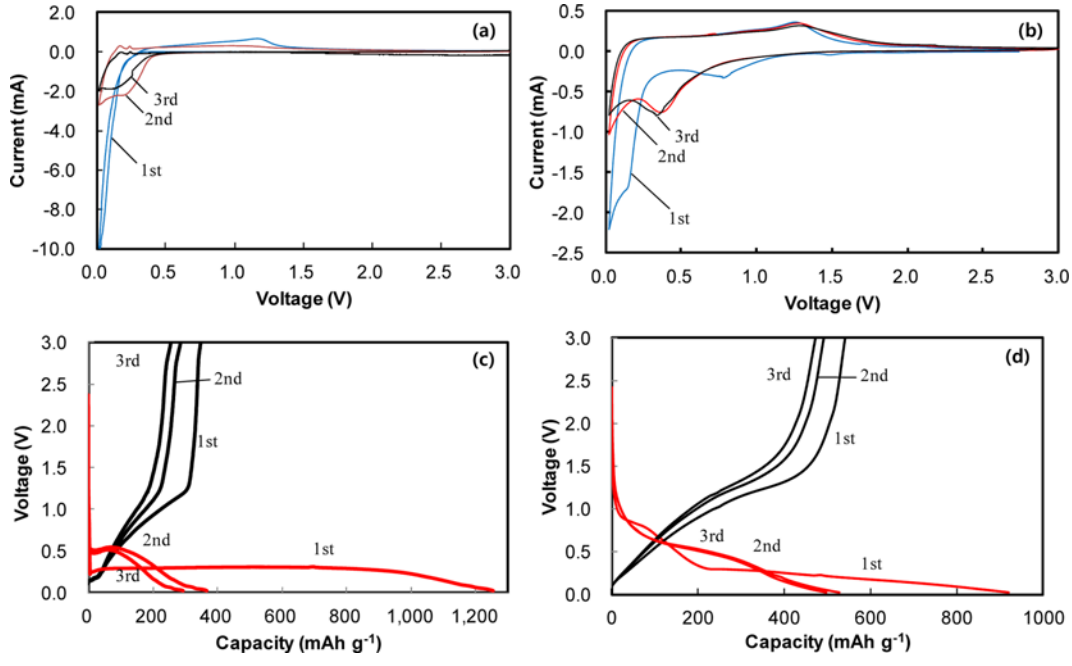

Fig. 5. Cyclic voltammograms of (a) Mn_3O_4 and (b) MnO/C at a scan rate of 0.1 mV s^{-1}, and discharge/charge voltage profiles of (c) Mn_3O_4 and (d) MnO/C at the current of 100 mA g^{-1}.

after the first cycle almost overlapped indicating much improved electrochemical reversibility of MnO/C compared with Mn_3O_4 electrode.

The corresponding voltage profiles of Mn_3O_4 and MnO/C composite obtained by galvanostatic cycling tests are shown in Fig. 5(c) and 5(d), respectively. In accordance with the CV profiles, the Mn_3O_4 electrode exhibited a rapid voltage drop followed by a long voltage plateau at 0.26 V giving a high specific capacity of 1,250 mAh g^{-1} in the first discharge process (Fig. 5(c)). The first discharge capacity was much higher than the theoretical one of Mn_3O_4 (936 mAh g^{-1}) estimated from the electrochemical conversion reaction (5) above possibly due to the well known interfacial lithium storage in the

Mn and Li_2O nano-grain boundaries [20,32] corresponding to the sloping voltage profile in the range of 0.2-0.01 V. However, the first charge capacity was only 380 mAh g^{-1} giving the Coulombic efficiency (CE) of 30.4%. Even in the subsequent cycles, the Mn_3O_4 electrode delivered the reversible capacity below 300 mAh g^{-1}. Both the low initial CE and low reversible capacity of Mn_3O_4 could be ascribed to the low intrinsic conductivity of Mn_3O_4 electrode and electrode pulverization caused by relatively large volume change during the conversion reaction process [31,33]. Fig. 5(d) shows the voltage profile for MnO/C composite. In the first discharge process, the voltage dropped rapidly down to 0.95 V followed by two plateaus at 0.95-0.33 V and 0.33-0.01 V corresponding to the SEI formation and Mn^{2+} reduction to Mn^0 as observed in the CV curve in Fig. 5(b). The voltage plateau at around 0.3 V in the first discharge curve was shifted to 0.6 V in the second cycle due to electrode polarization caused by irreversible phase transformation between crystalline MnO and Li_2O/Mn^0 [30]. The first discharge and charge capacities were 920 and 541 mAh g^{-1}, respectively, giving the first CE of 58.8%. The reversible capacity of 541 mAh g^{-1} for MnO/C composite is close to its theoretical capacity estimated by taking into account its MnO content as follows: 754 mAh g^{-1} (MnO capacity)×0.6+200 mAh g^{-1} (amorphous RF carbon capacity)×0.4=534 mAh g^{-1}.

Fig. 6 shows the cycling performances of Mn_3O_4 and MnO/C electrodes at the current of 100 or 200 mA g^{-1}. The MnO/C composite showed excellent cycling stability up to 103 cycles while the Mn_3O_4 electrode lost most of the capacity in 10 cycles. As evidenced in the TEM images of MnO/C composite in Fig. 4, MnO nanocrystals of 20-50 nm in diameter are well dispersed and encapsulated in carbon matrix. The unique nanostructure of MnO/C composite can provide conductive pathways in the electrode and efficiently absorb mechanical stresses associated with the volume changes of conversion reaction (2) above, which resulted in a superior cycling stability. Note that the capacity of MnO/C at 100 mA g^{-1} gradually increased with cycle number after about 50 cycles in agreement with other reports [20,34,35]. The origin was suggested to be related to the formation of high oxidation state products [20] or the reversible growth of a polymeric gel-like film caused by kinetically activated electrolyte degradation [35].

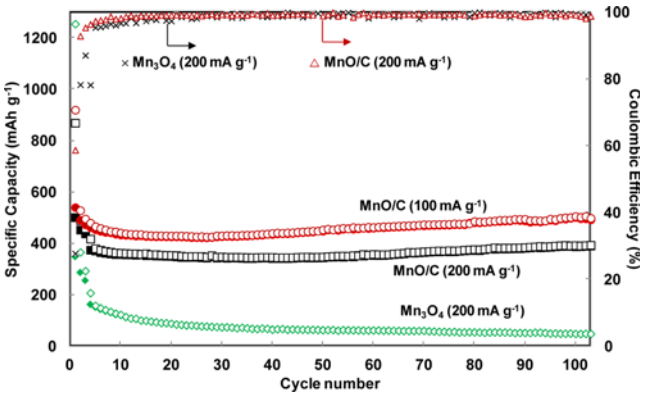

Fig. 6. Cycling performances of Mn_3O_4 and MnO/C at the cut-off voltage range of 0.01-3.0 V for 103 cycles (current is fixed at 100 mA g^{-1} for initial three cycles).

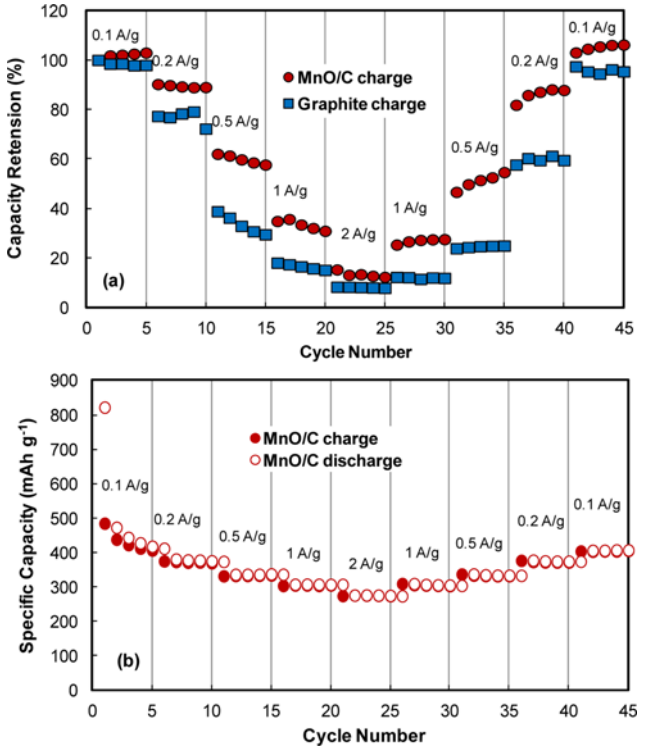

Fig. 7. (a) Comparison of rate responses of MnO/C and graphite when both charge and discharge currents are varied at the same time in the range of 100-2,000 mA g^{-1}, and (b) rate response of MnO/C at various discharge currents with a fixed charge current at 100 mA g^{-1}.

Finally, the rate capability of MnO/C composite was measured in comparison to that of commercial graphite anode at different current from 100 to 2,000 mA g^{-1}. Fig. 7(a) shows the relative charge capacity retentions of both MnO/C composite and graphite anodes at different current density to their base capacities at 100 mA g^{-1}. The currents for both charge and discharge cycles are varied at the same time. The capacity retentions for MnO/C anode were 90, 60 and 35% while those for graphite were 78, 33 and 17% on average at the currents of 200, 500 and 1,000 mA g^{-1}, respectively. Hence, the MnO/C possesses much higher rate capability than a commercial graphite anode. When the current was returned back to 100 mA g^{-1}, the capacity of MnO/C was completely restored after 45 cycles, indicating its excellent electrochemical reversibility. At relatively high currents of 1,000 and 2,000 mA g^{-1}, the capacity retentions were below 40%, suggesting relatively poor electrochemical conversion kinetics. To further test the discharge power capability of MnO/C, the discharge currents were varied over the range of 100-2,000 mA g^{-1} at the fixed charge current of 100 mA g^{-1}, the capacity retentions were as high as over 60% even at 2,000 mA g^{-1} as shown in Fig. 7(b), indicating a high discharge rate capability of MnO/C composite.

CONCLUSIONS

A facile synthesis strategy in which manganese oxide nanoparticle formation and carbon gel coating processes are combined in

a one-pot reaction was successfully demonstrated to prepare MnO/C nanocomposite. This synthesis approach eliminates the conventional processes of separate synthesis of manganese oxide nanostructures and additional steps of coating or hybridization with carbon. The as-prepared Mn_3O_4-carbon gel was converted into MnO/C (60 wt% MnO) composite in which 20-50 nm MnO nanoparticles were highly dispersed and encapsulated in carbon matrix after carbonization process. Thus obtained MnO/C composite exhibited the reversible capacity of 541 mAh g^{-1} at 100 mA g^{-1} with an excellent cycling stability up to 103 cycles. The MnO/C nanocomposite also showed much higher rate capability than a commercial graphite anode and delivered a discharge capacity around 300 mAh g^{-1} at the current as high as 2,000 mA g^{-1}. The MnO/C composite based on low cost materials and facile synthetic process could be an attractive candidate for large-scale energy storage applications.

ACKNOWLEDGEMENT

This work was supported by the National Research Foundation of Korea Grant funded by the Ministry of Education, Science and Technology (NRF-2012R1A1A2042487).

REFERNCES

1. P. L. Taberna, S. Mitra, P. Poizot, P. Simon and J.-M. Tarascon, *Nat. Mater.*, **5**, 567 (2006).
2. M. S. Whittingham, *MRS Bull.*, **33**, 411 (2008).
3. B. Scrosati and J. Garche, *J. Power Sources*, **195**, 2419 (2010).
4. J. Cabana, L. Monconduit, D. Larcher and M. R. Palacin, *Adv. Mater.,* **22**, E170 (2010).
5. J.-M. Tarascon, *Phil. Trans. R. Soc.*, **A368**, 3227 (2010).
6. C. Chae, H.-J. Noh, J. K. Lee, B. Scrosati and Y.-K. Sun, *Adv. Funct. Mater.*, (2014), DOI:10.1002/adfm.201303766.
7. P. Poizot, S. Laruelle, S. Grugeon, L. Dupont and J.-M. Tarascon, *Nature*, **407**, 496 (2000).
8. S.-S. Kim, *J. Korean Electrochem. Soc.*, **11**, 211 (2008).
9. H. Zhang, H. Tao, Y. Jiang, Z. Jiao, M. Wu and B. Zhao, *J. Power Sources,* **195**, 2950 (2010).
10. M.-Y. Cheng and B.-J. Hwang, *J. Power Sources*, **195**, 4977 (2010).
11. W. M. Zhang, X. L. Wu, J. S. Hu, Y. G. Guo and L. J. Wan, *Adv. Funct. Mater.*, **18**, 3941 (2008).
12. T. Yoon, C. Chae, Y. K. Sun, X. Zhao, H. H. Kung and J. K. Lee, *J. Mater. Chem.*, **21**, 17325 (2011).
13. H. L. Wang, L. F. Cui, Y. A. Yang, H. S. Casalongue, J. T. Robinson, Y. Y. Liang, Y. Cui and H. J. Dai, *J. Am. Chem. Soc.*, **132**, 13978 (2010).
14. P. Poizot, S. Laruelle, S. Grugeon and J.-M. Tarascon, *J. Electrochem. Soc.*, **149**, A1212 (2002).
15. C. Chae, J. H. Kim, J. M. Kim, Y.-K. Sun and J. K. Lee, *J. Mater. Chem.*, **22**, 17870 (2012).
16. T. Yoon, J. Kim, J. Kim and J. K. Lee, *Energies*, **6**, 4830 (2013).
17. C. Chae, H. Park, D. Kim, J. Kim, E.-S. Oh and J. K. Lee, *J. Power Sources*, **244**, 214 (2013).
18. C. W. Ahn, Y. H. Chung, B. D. Hahn, D. S. Park and Y. E. Sung, *Korean J. Chem. Eng.*, **29**, 985 (2012).
19. X. Fang, X. Lu, X. Guo, Y. Mao, Y.-S. Hu, J. Wang, Z. Wang, F. Wu, H. Liu and L. Chen, *Electrochem. Commun.*, **12**, 1520 (2010).
20. K. Zhong, X. Xia, B. Zhang, H. Li, Z. Wang and L. Chen, *J. Power Sources*, **195**, 3300 (2010).
21. K. F. Zhong, B. Zhang, S. H. Luo, W. Wen, H. Li, X. J. Huang and L. Q. Chen, *J. Power Sources*, **196**, 6802 (2011).
22. Y. He, L. Huang, J. S. Cai, X. M. Zheng and S. G. Sun, *Electrochim. Acta*, **55**, 1140 (2010).
23. P. C. Lian, X. F. Zhu, H. F. Xiang, Z. Li, W. S. Yang and H. H. Wang, *Electrochim. Acta*, **56**, 834 (2010).
24. M. Kang, E. D. Park, J. M. Kim and J. E. Yie, *Appl. Catal. A: Gen.*, **327**, 261 (2007).
25. Q. Feng, K. Yanagisawa and N. Yamasaki, *J. Porous Mater.*, **5**, 153 (1998).
26. S. Ching and J. L. Roark, *Chem. Mater.*, **9**, 750 (1997).
27. K. A. Malinger, Y.-S. Ding, S. Sithambaram, L. Espinal, S. Gomez and S. L. Suib, *J. Catal.*, **239**, 290 (2006).
28. J. Gao, M. A. Lowe and H. D. Abruna, *Chem. Mater.*, **23**, 3223 (2011).
29. Z. M. Cui, L. Y. Hang, W. G. Song and Y. G. Guo, *Chem. Mater.*, **21**, 1162 (2009).
30. B. Sun, Z. X. Chen, H. S. Kim, H. Ahn and G. X. Wang, *J. Power Sources*, **196**, 3346 (2011).
31. D. Pasero, N. Reeves and A. R. West, *J. Power Sources*, **141**, 156 (2005).
32. J. Jamnik and J. Maier, *Phys. Chem. Chem. Phys.*, **5**, 5215 (2003).
33. M. Au and T. Adams, *J. Mater. Res.*, **25**, 1649 (2010).
34. J. Li, H. M. Dahn, L. J. Krause, D. B. Le and J. R. Dahn, *J. Electrochem. Soc.*, **155**(11), A812 (2008).
35. G. Zhou, D. W. Wang, F. Li, L. Zhang, N. Li, Z. S. Wu, L. Wen, G. Q. Lu and H. M. Cheng, *Chem. Mater.*, **22**, 5306 (2010).